The Influence of Intrinsic Water and Ion Permeation on the Dielectric Properties of Parylene C Films

Jacob T. Pawlik [ORCID], *Member, IEEE*, Nikolas D. Barrera [ORCID], Eugene J. Yoon [ORCID], James C. Booth [ORCID], *Member, IEEE*, Christian J. Long [ORCID], Nathan D. Orloff [ORCID], *Senior Member, IEEE*, Ellis Meng [ORCID], *Fellow, IEEE*, and Angela C. Stelson [ORCID], *Member, IEEE*

Abstract—**Parylene C is a widely used dielectric barrier in implantable medical devices because it conforms well to surfaces and insulates against biological environments. However, multiple studies have shown that moisture can intrude into Parylene C films through defects and intrinsic diffusion, leading to delamination and device failure. While many studies have tested device integrity in vitro, few have isolated the influence of specific degradation mechanisms on device failure. Here, we use a broadband impedance technique called Microwave Microfluidic Spectroscopy (MMS) to measure fluid permeation in targeted regions of Parylene C films that are free of defects and have optimal adhesion to the substrate. We found no changes in the broadband S-parameters from 100 MHz–110 GHz for Parylene C coated coplanar waveguides soaked in water or phosphate buffered saline at 20 °C or 37 °C for two months. Furthermore, there was no delamination induced by fluid soaking. Our study helps to clear debate about the influence of water and ion diffusion on Parylene C device lifetime and inform better fabrication of Parylene C coatings for implantable devices.**

Index Terms—**Accelerated aging, delamination, dielectric measurements, implantable biomedical devices, microfluidics, microwave devices, polymer films, scattering parameters, spectroscopy.**

I. INTRODUCTION

IMPLANTABLE active medical devices provide a proximal interface to modulate biological systems [1]. These devices commonly employ polymer coatings to protect internalized devices from the harsh biological environment. Parylene C is a common choice for implantable device coatings because it is biocompatible, flexible, conformal, low-cost, easy to process and optically and RF transparent [2], [3]. Despite these advantages, Parylene C coatings are known to lose their barrier properties within months of operation in vivo, resulting in partial or complete device failure [4], [5]. Various mechanisms for barrier failure have been proposed, including oxidation, loss of adhesion to the substrate, permeation of fluid through pinhole defects and cracks, and intrinsic diffusion of water or ions through the film, leading to film delamination [6], [7], [8], [9], [10]. However, the influence of these individual degradation mechanisms on overall device lifetime is unclear, which slows the improvement of Parylene C-based devices. Resolving coating failure mechanisms may lead to increased lifetime of implanted medical devices and reduction of costly, invasive follow-up procedures for patients.

Many studies have explored the failure mechanisms of Parylene C coatings, but few isolate the effects of specific degradation pathways on device performance. While in vivo studies certainly reflect the true integrity of implantable devices [4], [5], they are costly and time-consuming. A less costly method is to use electrochemical impedance spectroscopy (EIS) (0.1 Hz–1 MHz) in combination with in vitro accelerated aging to evaluate the lifetime of Parylene C devices [4], [5], [10], [11], [12], [13]. Devices are soaked at elevated temperatures in biological environments (*e.g.*, phosphate-buffered saline, PBS), then the device impedance is monitored over time. In this case, a change in impedance indicates device failure. The lifetime of the device can be extrapolated down to body temperature (37 °C) by an Arrhenius model [9].

However, device performance at elevated temperatures is not always reflective of behavior at 37 °C, because the acquired data is above the glass transition temperature of Parylene C (∼50 °C) [11], [14]. Moreover, EIS frequency windows are often narrow, and the complexity of equivalent circuit modeling makes it difficult to assign impedance changes to specific degradation mechanisms [7], [9], [10]. EIS may exclude important fluid effects that can be indicative of device failure, such as changes in ionic conductivity, ion pairing, or molecular relaxations that occur at much higher frequencies (1 MHz–1 THz) [15]. Given the ambiguity in the literature, we sought to test if microwave microfluidic spectroscopy (MMS) might provide additional information that could help isolate the effects of individual degradation mechanisms on Parylene C device performance.

Microwave Microfluidic Spectroscopy (MMS) is a dielectric spectroscopy technique used to characterize fluids over a broad range of frequencies (40 kHz–110 GHz) [16], [17], [18]. MMS uses measured scattering parameters (S-parameters) of coplanar waveguides covered with microfluidic channels. Electromagnetic modeling is used to fit the S-parameter data to equivalent
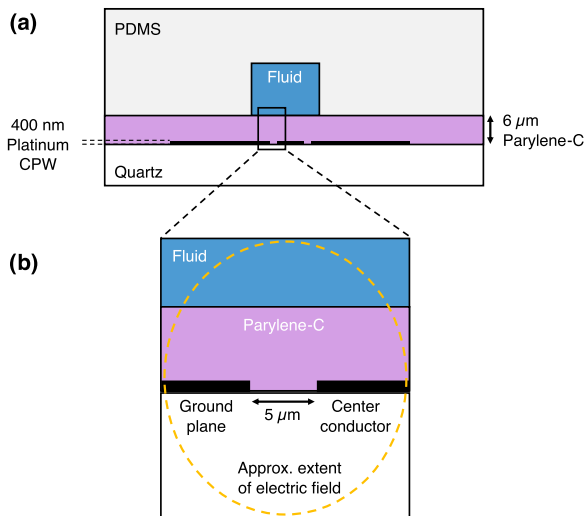
Fig. 1.   Microwave microfluidics device used to measure water and ion permeation in Parylene C films. (a) Cross-section of the Parylene C device. (b) Zoom-in of the interelectrode gap where the electric field is concentrated.

circuit models and extract dielectric properties. This technique captures many dielectric effects in one measurement, including electric double layer formation, ionic conduction, ion pairing, and dipolar relaxations [17], [19]. With MMS, we can track the presence of water or ions directly by analyzing their dielectric responses at higher frequencies.

Changes in Parylene C film integrity through oxidation, permeation into defects, and poor adhesion is well studied [5], [6], [7], [11]. Here, we are interested in determining whether intrinsic water and ion permeation through Parylene C films can induce film delamination in absence of other failure mechanisms. Few studies have explored intrinsic fluid permeation into Parylene C. Davis, et al. observed diffusion of water into Parylene C (6.2 $\times$ 10^{-9} cm^2/s) within days of soaking at 25 °C by infrared spectroscopy [20]. Song, et. al. observed significant permeation of water and Na$^+$ ions through Parylene C coatings on transistor devices at 95 °C [21]. However, neither study correlated intrinsic diffusion with film failure at realistic conditions (37 °C). Here, we perform an experiment that isolates the effect of intrinsic fluid permeation on Parylene C film failure at 37 °C in the absence of other failure modes.

In what follows, we use MMS to measure the effects of intrinsic water and ion permeation on Parylene C film dielectric and structural properties. We can isolate the intrinsic diffusion by analyzing microscopic regions of the film that are free of defects and have good adhesion to the substrate. Microfluidics helped mitigate edge effects during the fluid soaking that can make it difficult to study intrinsic fluid permeation into the polymer film. We measured the broadband S-parameters (100 MHz–110 GHz) of Parylene C coated coplanar waveguides (CPWs) soaked in H$_2$O or 1×PBS at 20 °C or 37 °C for a two-month period (Fig. 1). Changes in S-parameters were used as a proxy for the diffusion of water and ions into the film. We found that the S-parameters of fluid-soaked Parylene C devices did not change significantly over the two-month period, indicating that only a small amount of water and ions permeated into the film. Also, profilometry
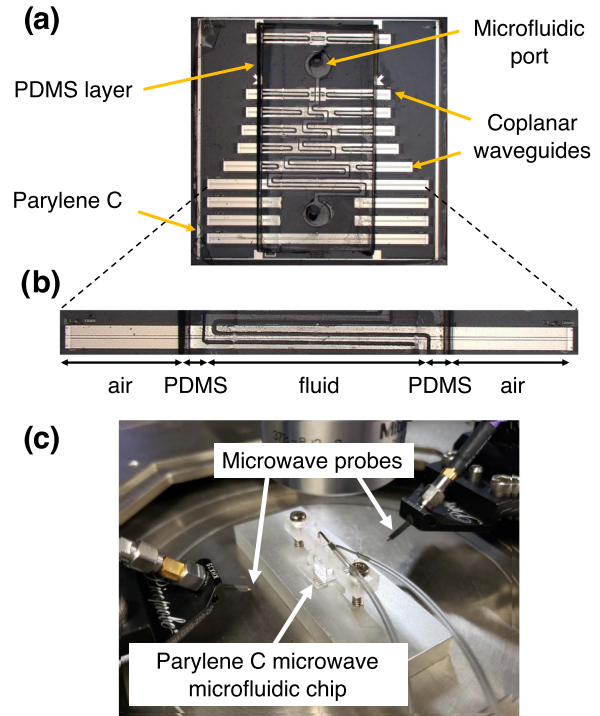

Fig. 2.   Parylene C microwave microfluidic chip. (a) Parylene C chip with PDMS microfluidic layer aligned on top. (b) Zoom-in of the Parylene C device, showing a single coplanar waveguide. (c) Assembled Parylene C microfluidic chip on a probe station.

and imaging showed no signs of delamination or cracking of the films. Therefore, we find that water and ion permeation is unlikely to cause significant changes in Parylene C film properties in biological environments. Below, we outline our experimental progression and measurement results to support these conclusions.

II. PARYLENE C DEVICE FABRICATION

A. Chip Fabrication

We used procedures outlined by Yoon et al. to fabricate Parylene C coated platinum coplanar waveguides (Pt CPWs) on a fused silica wafer (Supplemental I) [22]. The fabricated wafer was annealed at 200 °C for 48 hours in a N$_2$ gas purged vacuum oven to improve the crystallinity and adhesion of the Parylene C films [8]. We also fabricated reference chips with Au CPWs to calibrate S-parameter data to the probe tips of the microwave probes (described in Section IV-A) [19].

Next, we fabricated a polydimethylsiloxane (PDMS) microfluidic cover via mold casting in a 3D-printed mold, which had microfluidic channels on the bottom measuring 213 μm ($\pm$3 μm) wide by ∼100 μm deep. Fig. 2(a) shows the PDMS cover aligned on the Parylene C chip. We chose Parylene C chips that were free of debris and macroscopic defects for device assembly. Fig. 2(b) shows an example of a Parylene C device. The total line lengths and channel lengths of the Parylene C devices we measured are given in Table I. Fig. 2(c) shows the assembled chip on our microwave measurement probe station.

TABLE I
EXPERIMENTAL CONDITIONS FOR SOAKED PARYLENE C DEVICES

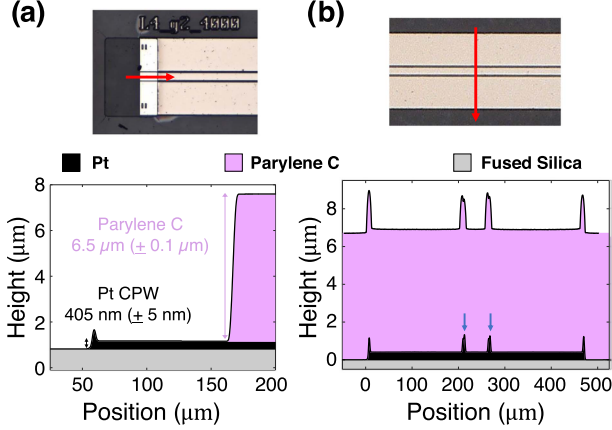| Fluid condition	Line length (mm)	Channel length (mm)	Measurement days
H_2O, 20°C	6.5	2.695	0, 1, 7, 56
1×PBS, 20°C	10.0	4.160	1, 28, 56
1×PBS, 37°C	10.0	4.160	0, 7, 28, 56

(a) **(b)**

Fig. 3. Stylus profilometry of Parylene C devices. Red arrow indicates the scan direction. (a) Line profile at the Pt CPW landing pad. (b) Line profile of the Pt CPW cross section with and without Parylene C on top. Blue arrows indicate the approximate position of the CPW gaps. We observe fencing of the Pt at edges and the Parylene C film conforms to these Pt features.

B. Measurements of Device Geometry

We measured the topography of the Parylene C devices with a stylus profilometer. With this data, we constructed accurate electromagnetic models of the device geometry and set a baseline for the device form factor. The stylus had a force of 2 mg and a scan speed of 5 μm/s at a 200 Hz tapping frequency. Fig. 3(a) shows a line profile of the cutout region in the Parylene C film that starts at the substrate level and progresses onto the Pt CPW and Parylene. From left to right, the first feature is a protrusion at the Pt CPW edge. The edge is raised by an additional 0.5 μm above the plane of the Pt CPW and is likely a result of inconsistent removal of metal at the edges during the lift-off process, leaving behind Pt "fences" [23], [24]. The Pt thickness was 405 nm ($\pm$5 nm), close to the intended thickness of 400 nm. The Parylene C edge had an average height of 6.5 μm ($\pm$0.1 μm), close to the intended thickness of 6 μm.

A profile of a Parylene C coated CPW in Fig. 3(b) shows protrusions directly above the Pt fences, indicating that the Parylene C film conformed well to the Pt topography. The size of the protrusions (1.8 μm $\pm$ 0.2 μm) is much larger than the Pt fences, which may be a result of the added thickness from the Parylene C film conformal deposition. While metal fencing can sometimes impact device performance, we ensured the functionality of each Parylene C device with S-parameter measurements (see Section IV). We also accounted for the protrusions in the Parylene C in our electromagnetic simulations to accurately model the device.
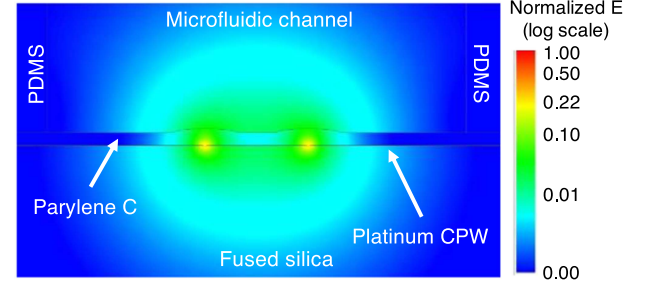

Fig. 4. 2D electromagnetic simulation at 50 GHz of a Parylene C coated CPW with the PDMS microfluidics at the channel section. The intensity of the electric field generated by the CPW is given as a gradient log scale on the right. The electric field is most concentrated in the interelectrode gap, but penetrates through the entire thickness of Parylene C.

III. ELECTROMAGNETIC SIMULATIONS
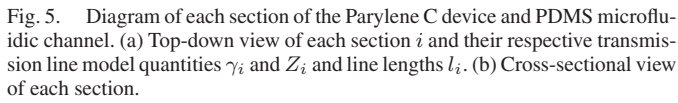
A. Electric Field Simulation

We performed 2D electromagnetic simulations to model the dielectric properties of the Parylene C device with different fluids (air, water, or 1×PBS) in the microfluidic channel. The permittivity and conductivity values assigned to each material are listed in Supplemental IIA. We determined the dimensions for the model from stylus profilometry and optical imaging. These simulations produced distributed circuit parameters that we used to build S-parameter models with varying material properties but the same measured cross-sectional geometry. Due to the constraints of the device design, constructing the S-parameters of the full device in simulation and comparing them to experimental S-parameters is necessary to validate our dielectric model and estimate the material properties of Parylene C.

We plot the simulated 2D electric field generated in the channel region of the Parylene C device at 50 GHz in Fig. 4. The electric field penetrates through the Parylene C film and extends into the fluid above. Since most of the electric field is concentrated in the Parylene C film near the interelectrode gap, our measurements are more sensitive to dielectric changes in this region compared to the rest of the device. The magnitude of the electric field diminishes by only one order of magnitude through the Parylene C film, indicating we maintain sensitivity to dielectric changes throughout the entire film thickness. We also compared the electric field distributions with varying permittivity of the Parylene C to simulate the effects of fluid intrusion on the confinement of the electric field. As shown in Fig. S2, the electric field distribution does not change significantly, indicating that we maintain sensitivity throughout the entire thickness of Parylene C even as the permittivity changes.

B. S-Parameter Simulations

Our electromagnetic simulations predict the S-parameters of the Parylene C device for each fluid condition and establish the sensitivity of our measurements. We simulate the S-parameters calibrated to the probe tips by cascading individual sections of the Parylene C device (Fig. 5) using methods outlined in [18]. From simulations, we derived the transmission line circuit model elements R_i, L_i, C_i, and G_i for each section i of the line in

Fig. 5. Diagram of each section of the Parylene C device and PDMS microfluidic channel. (a) Top-down view of each section i and their respective transmission line model quantities γ_i and Z_i and line lengths l_i. (b) Cross-sectional view of each section.

Fig. 6. Comparison between simulated and experimental S-parameters for Parylene C devices filled with air, H_2O, or $1\times$PBS at 20 °C at day 0. Panels a,c give the linear magnitude of S_{11} and S_{21} with measurement uncertainty (indicated by line thickness), while panels b,d give the difference between the simulated and experimental S-parameters for S_{11} and S_{21}, respectively. The experimental S-parameters agree well with simulated values and differences are of similar magnitude to the measurement uncertainty.

Fig. 5, then we computed the characteristic impedance Z_i and propagation constant γ_i of each section i:

$$Z_i = \frac{\sqrt{R_i + i\omega L_i}}{\sqrt{G_i + i\omega C_i}} \qquad (1)$$

$$\gamma_i = \sqrt{(R_i + i\omega L_i)(G_i + i\omega C_i)} \qquad (2)$$

Given the Z_i and γ_i of each section, we derived the transmission parameter matrix T_i of each section and the impedance transformers $Q_{Z_m}^{Z_n}$ for each transition of Z_i between sections:

$$T_i = \begin{bmatrix} e^{-\gamma_i l_i} & 0 \\ 0 & e^{\gamma_i l_i} \end{bmatrix} \qquad (3)$$

$$Q_{Z_m}^{Z_n} = \frac{1}{2Z_m} \left| \frac{Z_m}{Z_n} \right| \sqrt{\frac{Re(Z_n)}{Re(Z_m)}} \begin{pmatrix} Z_n + Z_m & Z_n - Z_m \\ Z_n - Z_m & Z_n + Z_m \end{pmatrix} \qquad (4)$$

where n and m denote transmission of a signal from section n to section m. We then computed a T-matrix T_{all} representing the entire device in Fig. 5(a), corrected to 50 Ω by cascading the T-matrices and Q-matrices as follows:

$$T_{all} = Q_1^{50\Omega} T_1 Q_2^1 T_2 Q_3^2 T_3 Q_4^3 T_4 Q_3^4 T_3 Q_2^3 T_2 Q_1^2 T_1 Q_{50\Omega}^1 \qquad (5)$$

where indices of each matrix correspond to section numbers labelled in Fig. 5(a).

We converted T-matrices to S-parameters, then plotted the result as a function of frequency. We show the simulated S-parameters for a Parylene C device filled with air, H_2O, or $1\times$PBS solution in Fig. 6. S_{11} and S_{21} represent the reflection and transmission of the microwave signal from the Parylene C device, respectively. Each fluid gives unique S-parameters across the entire frequency range. The magnitude of the S-parameters drops at around 1 GHz due to the skin effect, where the electric field becomes confined to the surface of the conductor at higher frequencies [25]. $1\times$PBS shows greater attenuation of the microwave signal compared to H_2O, likely due to the higher ionic conductivity of the $1\times$PBS solution. There are also differences in the curvature of S_{11} around 10 GHz, which is in the frequency range of dielectric loss for water [17]. This simulation shows that our electrical measurements are sensitive to dielectric changes unique to each fluid in the channel region.
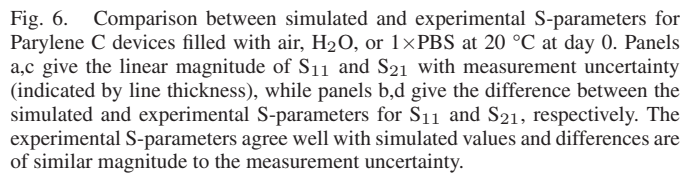
To further assess our measurement sensitivity, we performed simulations where we altered the dielectric constant of Parylene C in the channel region and quantified changes to the overall S-parameters (Fig. S3). We find that $|S_{11}|$ is sensitive to changes in the Parylene C dielectric constant as small as ± 0.2 near 10 GHz, while $|S_{21}|$ is less sensitive (± 0.8 near 10 GHz). Furthermore, we simulated the effects of film delamination by removing Parylene C entirely from the channel region (Fig. S4). In Fig. S5, we observe distinct changes in both $|S_{11}|$ and $|S_{21}|$ across all frequencies. Preliminary results from additional simulations of minor delamination (by introduction of small air gaps) indicate that our measurements are sensitive to just 50 nm of film separation [26]. Our S-parameter measurements are highly sensitive to dielectric changes in the Parylene C film and to film delamination.

IV. S-PARAMETER MEASUREMENTS

A. Comparison of Experimental and Simulated Data

We obtained S-parameter measurements with a vector network analyzer (VNA) and extender heads on a temperature-controlled probe station. We measured 512 frequency points on a log grid from 100 MHz to 110 GHz with a 10 Hz intermediate frequency bandwidth and source power of -17 dBm. All S-parameter measurements were calibrated to the probe tips with a combination of multiline thru-reflect-line (TRL) and series resistor calibrations [27], leaving only the Parylene C device as the device under test. We performed S-parameter calibrations and sensitivity analysis with the NIST Microwave Uncertainty Framework using the "elaborate closed-form coplanar waveguide transmission line" model [28]. The upper and lower 95% confidence intervals for S-parameter values were determined from sensitivity analysis and the results were implemented as type B uncertainty. We estimated the type A uncertainty of our measurements by taking the standard deviation of measurements on the same Pt CPW across eight different calibrations. The
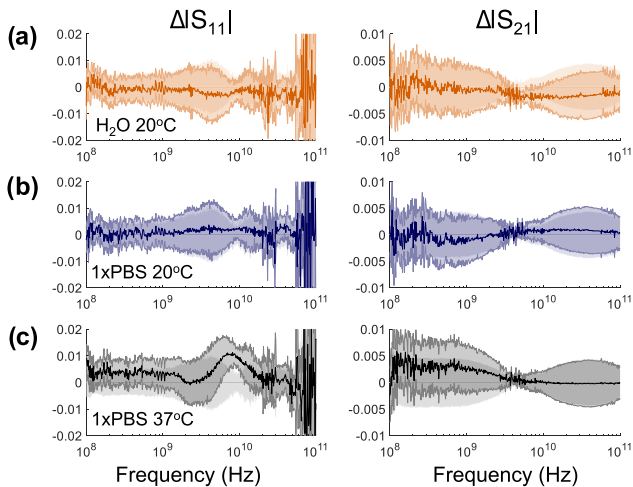
Fig. 7.   Differences in the linear magnitude of S_{11} and S_{21} between day 0 and day 56 for Parylene C devices soaked in (a) H_2O at 20 °C, (b) 1×PBS at 20 °C, and (c) 1×PBS at 37 °C for 2 months. The uncertainty bounds are given as a shaded region on the day 56 curve and also on the x-axis as a reference for day 0. Overall, we observe no significant changes in S-parameters for any of the fluid conditions.

uncertainties were compiled from each analysis into a single uncertainty by a root mean square sum. The uncertainty for day 0 measurements of 1×PBS are reported with a 95% confidence interval in Fig. 6(b) and (d) as a reference for the accuracy of our simulated S-parameters.

In Fig. 6, we compare the linear magnitude of experimental and simulated S-parameters of Parylene C devices filled with air, water, or 1×PBS at 20 °C. For each case, the S-parameters are dampened at frequencies > 1 GHz due to the skin effect, which is the confinement of electric current to the surface of the Pt CPW at high frequencies. The differences in S-parameters for each fluid condition are small at low frequencies and increase only slightly at higher frequencies. We observed similar agreement in the phase data (Fig. S8). These small differences indicate a close match in the anticipated geometry and material properties of the simulation to the physical setup. Remaining differences are likely a result of non-idealities such as surface roughness, Pt fencing, channel misalignment, and variation of thickness along the length of the device.

B. S-Parameters of Soaked Parylene C Devices

We measured the S-parameters of Parylene C devices soaked in different fluid conditions to capture changes in the dielectric properties of the film over time. We focus on measurements of air-filled devices since the simulations agreed with experiments most accurately when the properties of the fluid were omitted. In this way, we can isolate changes in the dielectric properties of the Parylene C film irrespective of changes in the fluid over time. We obtained measurements of the air-filled channel by removing the fluid, washing with deionized water, and drying the microfluidic channel with a syringe. We also replenished fluid levels as needed to retain a consistent volume and steady conditions in the microfluidic lines.

Fig. 7 shows the differences in linear magnitude of S_{11} and S_{21} on day 56 compared to the first measurement day for

each fluid condition. The data for each fluid condition shows that the differences in S-parameters from day 0 to day 56 are not significantly different from the typical repeatability of our measurements. There were some slight differences in S_{11} near 10 GHz for the 1×PBS device at 37 °C, where our measurements are most sensitive, but the data does not significantly exceed the measurement uncertainty bounds from previous days and does not display a trend over time. We also observe no changes in the phase for each fluid condition (Fig. S9). Given the high sensitivity of our measurements to dielectric changes in the Parylene C, we conclude that soaking Parylene C films in H_2O or 1×PBS at 20 °C or 37 °C does not induce significant coating failure. If significant delamination had occurred, we would have observed drastic changes in $|S_{11}|$ and $|S_{21}|$, exceeding the uncertainty threshold of ± 0.01. Moreover, it is likely that water and ion permeation does not occur substantially in our films under these conditions.

V. DEVICE CHARACTERIZATION AFTER SOAKING

A. Optical Imaging

We obtained optical images of the devices after soaking to capture macroscopic changes in the device form factor (Fig. S10). For the H_2O chip, we observe clear differences in the quality of the Parylene C in the channel region compared to the rest of the Parylene C film. Near the interelectrode gap region, the Parylene C has a lighter tint than the surrounding material. This change may indicate some disruption to the adhesion of the Parylene C film to the Pt CPW near the electrode edges. However, this film disruption was not observed on any of the other fluid soaked CPWs on the chip (Fig. S11). Also, we soaked a separate Parylene C device in D_2O for 1 month and observed no disruption of the Parylene C film (Fig. S12). This suggests that the Parylene C film was already in this state before soaking. Unlike the H_2O-soaked chip, the Parylene C films soaked in 1×PBS showed no signs of delamination. Since 1×PBS at 37 °C is a more intense soaking condition than H_2O at 20 °C, the delamination at the electrode edge in the H_2O device is likely an anomaly. The optical imaging shows that the fluids did not induce macroscopic changes to the Parylene C film properties, corroborating our S-parameter measurements.

B. Stylus Profilometry

Fig. 8 shows cross-sectional profiles of the channel regions of the Parylene C devices soaked in each fluid. A comparison of profiles between an unsoaked device and soaked devices shows that there are minimal changes to the physical topography after 56 days for the 1×PBS devices. Meanwhile, the H_2O profiles show broadening at the base of the protrusions at the interelectrode gaps, reaching ∼60 μm compared to the 20 μm–30 μm peak width for the other profiles. Again, since 1×PBS is a more intense soaking condition than H_2O, we suspect that the delamination in the H_2O device was anomalous and present before the soaking experiment. We also observe no broadening of the protrusions in the D_2O profile after 1 month of soaking. Overall, the fluid conditions did not cause major disruption or delamination of the Parylene C films in our devices. We find that
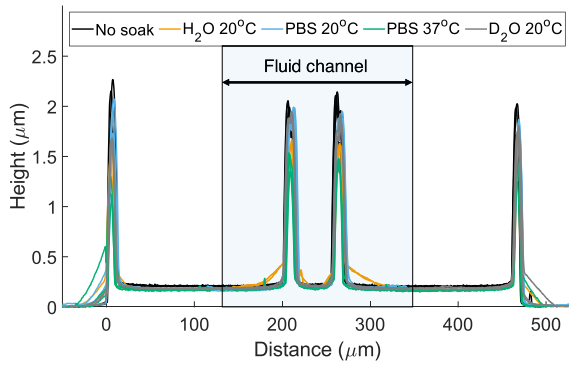
Fig. 8. Stylus profilometry of Parylene C devices after soaking in fluid (see Table I). Each sample includes three different measurements overlayed. While the H_2O profile does show some irregularities near the interelectrode gap, the overall topography of each Parylene C device did not change significantly. Also, the D_2O profile shows no deformation after soaking.

the intrinsic permeation of water and ions into Parylene C films does not cause a significant loss in structural integrity or volume change in the absence of macroscopic defects.

VI. DISCUSSION

Our results are consistent with some prior reports of Parylene C device lifetimes in phosphate-buffered saline at 37 °C, which are typically > 1 year [13], [29], [30], [31]. We find this to be especially true for ~5 μm Parylene C films that were prepared with optimal adhesion to the substrate and were free of defects. Multiple studies have shown that introducing the adhesion promoter A-174 silane [32], [33] or annealing Parylene C films above 200 °C in an inert atmosphere [8], [20], [29] significantly improves film adhesion and fluid barrier properties. Without any surface treatments or annealing, Parylene C films have been known to fail within days of soaking [13], [29]. We annealed our Parylene C films at 200 °C for 48 hours under vacuum to improve adhesion to the Pt surface and enhance the barrier properties. We also ensured the absence of macroscopic defects on the Parylene C surface before measurements. Proper adhesion and defect-free deposition of Parylene C films is pertinent for ensuring device longevity.

Given the repeated success of annealed Parylene C devices in saline at 37 °C, our results are not initially surprising. However, no study had yet investigated the influence of fluid permeation on Parylene C device lifetime in the absence of defects and with good film adhesion. Many studies submerge an entire Parylene C device into fluid and measure the impedance over time. With MMS, we were able to simplify the equivalent circuit model to a microscopic region of the Parylene C film free of defects. This allowed us to better isolate the influence of intrinsic permeation on coating failure. Our study confirms that intrinsic fluid permeation does not give rise to coating failure in 1×PBS at 37 °C in a 2-month period.

Although we were not able to directly measure a fluid permeation rate of water or ions through Parylene C, we can conclude that the fluid saturation point is small given the consistency of our S-parameter measurements over a two-month period. Water permeation measurements performed by Davis, et al. show evidence of diffusion of water into Parylene C within

days of soaking (6.2×10^{-9} cm^2/s), reaching a saturation point of ~ 0.5 wt% after 1 month for a 17 μm thick film [20]. Our S-parameter measurements were likely not sensitive enough to detect the ultralow concentrations of water reported in these studies. However, our research focus was instead to determine effects of soaking on coating failure. Our findings show that the overall water absorption into Parylene C had minimal effect on the coating quality and electrical properties of the film. Resonant or interferometric techniques focused on a single frequency might improve the sensitivity to detect permeation beyond what was demonstrated here.

While the purpose of this study was to isolate the influence of fluid permeation on Parylene C device performance, we acknowledge that our measurements do not reflect the actual environment of an implanted Parylene C device. in vivo experiments show highly accelerated Parylene C coating failure compared to in vitro studies, attributable to the harsh oxidative environment of the body [5], [11]. Soaking Parylene C devices in phosphate-buffered saline at 37 °C does not directly translate to device lifetime in vivo. Some studies have achieved greater parity between in vivo and in vitro experiments by introducing oxidative species such as H_2O_2 into the measurement setup [5], [11]. In addition, implantable devices often operate under mechanical stress and active voltage or current conditions, which can accelerate device failure [34]. Given the convenience of performing in vitro studies to predict implantable Parylene C device lifetime, more research is needed on artificial conditions that closely mimic the biological environment of the body.

VII. CONCLUSION

In this study, we employed Microwave Microfluidic Spectroscopy (MMS) to examine the effects of fluid permeation on Parylene C film dielectric and structural properties. We measured the broadband dielectric properties of Parylene C devices (100 MHz–110 GHz) subjected to biological-like conditions (1×PBS at 37 °C) over a two-month period and observed no measurable changes in the S-parameters. Additionally, we did not observe delamination or other significant structural changes in the Parylene C film. This suggests that the loss of barrier properties of Parylene C films in medical devices does not occur solely from intrinsic bulk fluid or ion permeation. For future studies, we suggest that Parylene C medical device testing should focus on assessing other modes of fluid-induced delamination, such as fluid transport through defects. Each of these failure mechanisms is likely to depend on variations in topography, film thickness, and surface area. Also, improved accuracy of equivalent circuit models for complicated device geometries will improve understanding of potential Parylene C film failure mechanisms. Broadly, this work provides valuable context for extending implanted medical device longevity and enhancing the quality of life for patients.

REFERENCES

[1] K. Bazaka and M. V. Jacob, "Implantable devices: Issues and challenges," *Electronics*, vol. 2, no. 1, pp. 1–34, Dec. 2012, doi: 10.3390/electronics2010001.

[2] Y. Qin, M. M. R. Howlader, M. J. Deen, Y. M. Haddara, and P. R. Selvaganapathy, "Polymer integration for packaging of implantable sensors," *Sensors Actuators B Chem.*, vol. 202, pp. 758–778, Oct. 2014, doi: 10.1016/j.snb.2014.05.063.

[3] M. Golda-Cepa, K. Engvall, M. Hakkarainen, and A. Kotarba, "Recent progress on Parylene C polymer for biomedical applications: A review," *Prog. Org. Coatings*, vol. 140, Mar. 2020, Art. no. 105493, doi: 10.1016/j.porgcoat.2019.105493.

[4] A. Lecomte, E. Degache, E. Descamps, L. Dahan, and C. Bergaud, "In vitro and in vivo biostability assessment of chronically-implanted Parylene C neural sensors," *Sensors Actuators B Chem.*, vol. 251, pp. 1001–1008, 2017, doi: 10.1016/j.snb.2017.05.057i.

[5] R. Caldwell, M. G. Street, R. Sharma, P. Takmakov, B. Baker, and L. Rieth, "Characterization of Parylene-C degradation mechanisms: In vitro reactive accelerated aging model compared to multiyear in vivo implantation," *Biomaterials*, vol. 232, Feb. 2020, Art. no. 119731, doi: 10.1016/j.biomaterials.2019.119731.

[6] D. Zeniieh, A. Bajwa, L. Ledernez, and G. Urban, "Effect of plasma treatments and plasma-polymerized films on the adhesion of Parylene-C to substrates," *Plasma Processes Polymers*, vol. 10, no. 12, pp. 1081–1089, Dec. 2013, doi: 10.1002/ppap.201300045.

[7] J. Ortigoza-Diaz et al., "Techniques and considerations in the microfabrication of Parylene C microelectromechanical systems," *Micromachines*, vol. 9, no. 9, 2018, Art. no. 422, doi: 10.3390/mi9090422.

[8] J. Ortigoza-Diaz, K. Scholten, and E. Meng, "Characterization and modification of adhesion in dry and wet environments in thin-film Parylene systems," *J. Microelectromech. Syst.*, vol. 27, no. 5, pp. 874–885, 2018, doi: 10.1109/JMEMS.2018.2854636.

[9] R. Caldwell, H. Mandal, R. Sharma, F. Solzbacher, P. Tathireddy, and L. Rieth, "Analysis of Al_2O_3-Parylene C bilayer coatings and impact of microelectrode topography on long term stability of implantable neural arrays," *J. Neural Eng.*, vol. 14, no. 4, 2017, Art. no. 046011, doi: 10.1088/1741-2552/aa69d3.

[10] W. Chun, N. Chou, S. Cho, S. Yang, and S. Kim, "Evaluation of sub-micrometer Parylene C films as an insulation layer using electrochemical impedance spectroscopy," *Prog. Org. Coatings*, vol. 77, no. 2, pp. 537–547, Feb. 2014, doi: 10.1016/j.porgcoat.2013.11.020.

[11] P. Takmakov, K. Ruda, K. S. Phillips, I. S. Isayeva, V. Krauthamer, and C. G. Welle, "Rapid evaluation of the durability of cortical neural implants using accelerated aging with reactive oxygen species," *J. Neural Eng.*, vol. 12, no. 2, 2015, Art. no. 026003, doi: 10.1088/1741-2560/12/2/026003.

[12] S. Minnikanti et al., "Lifetime assessment of atomic-layer-deposited Al_2O_3-Parylene C bilayer coating for neural interfaces using accelerated age testing and electrochemical characterization," *Acta Biomaterialia*, vol. 10, no. 2, pp. 960–967, 2014, doi: 10.1016/j.actbio.2013.10.031.

[13] J. P. Seymour, Y. M. Elkasabi, H. Y. Chen, J. Lahann, and D. R. Kipke, "The insulation performance of reactive parylene films in implantable electronic devices," *Biomaterials*, vol. 30, no. 31, pp. 6158–6167, 2009, doi: 10.1016/j.biomaterials.2009.07.061.

[14] J. J. Senkevich, B. W. Woods, J. J. McMahon, and P. I. Wang, "Thermomechanical properties of parylene X, A room-temperature chemical vapor depositable crosslinkable polymer," *Chem. Vapor Deposition*, vol. 13, no. 1, pp. 55–59, Jan. 2007, doi: 10.1002/cvde.200606541.

[15] W. H. H. Woodward, "Broadband dielectric spectroscopy–A practical guide," in *Broadband Dielectric Spectroscopy: A Modern Analytical Technique* (ACS Symposium Series), vol. 1375. Washington, DC, USA: American Chemical Society, 2021, pp. 3–59, doi: 10.1021/bk-2021-1375.ch001.

[16] A. C. Stelson et al., "Measuring ion-pairing and hydration in variable charge supramolecular cages with microwave microfluidics," *Commun. Chem.*, vol. 2, no. 54, pp. 1–10, 2019, doi: 10.1038/s42004-019-0157-9.

[17] C. A. E. Little, A. C. Stelson, N. D. Orloff, C. J. Long, and J. C. Booth, "Measurement of ion-pairing interactions in buffer solutions with microwave microfluidics," *IEEE J. Electromagn., RF Microw. Med. Biol.*, vol. 3, no. 3, pp. 184–190, Sep. 2019, doi: 10.1109/JERM.2019.2896719.

[18] J. C. Booth, N. D. Orloff, J. Mateu, M. Janezic, M. Rinehart, and J. A. Beall, "Quantitative permittivity measurements of nanoliter liquid volumes in microfluidic channels to 40 GHz," *IEEE Trans. Instrum Meas.*, vol. 59, no. 12, pp. 3279–3288, Dec. 2010, doi: 10.1109/TIM.2010.2047141.

[19] C. A. E. Little, N. D. Orloff, I. E. Hanemann, C. J. Long, V. M. Bright, and J. C. Booth, "Modeling electrical double-layer effects for microfluidic impedance spectroscopy from 100 kHz to 110 GHz," *Lab Chip*, vol. 17, 2017, Art. no. 2674, doi: 10.1039/c7lc00347a.

[20] E. M. Davis, N. M. Benetatos, W. F. Regnault, K. I. Winey, and Y. A. Elabd, "The influence of thermal history on structure and water transport in Parylene C coatings," *Polymer*, vol. 52, no. 23, pp. 5378–5386, Oct. 2011, doi: 10.1016/j.polymer.2011.08.010.

[21] E. Song et al., "Ultrathin trilayer assemblies as long-lived barriers against water and ion penetration in flexible bioelectronic systems," *Amer. Chem. Soc. Nano*, vol. 12, no. 10, pp. 10317–10326, 2018, doi: 10.1021/acsnano.8b05552.

[22] E. J. Yoon, A. C. Stelson, N. D. Orloff, C. J. Long, J. C. Booth, and E. F. Meng, "The effect of annealing thin film Parylene C-platinum interfaces characterized by broadband dielectric spectroscopy," in *Proc. IEEE 21st Int. Conf. Solid-State Sensors, Actuators Micro-Syst. (Transducers)*, 2021, pp. 884–887, doi: 10.1109/Transducers50396.2021.9495440.

[23] E. M. Preiss, A. Krauss, and H. Seidel, "Sputtered Pt electrode structures with smoothly tapered edges by bi-layer resist lift-off," *Thin Solid Films*, vol. 597, pp. 158–164, 2015, doi: 10.1016/j.tsf.2015.11.026.

[24] D. Berkoh and S. Kulkarni, "Challenges in lift-off process using CAMP negative photoresist in III-V IC fabrication," *IEEE Trans. Semicond. Manuf.*, vol. 32, no. 4, pp. 513–517, Nov. 2019, doi: 10.1109/TSM.2019.2944133.

[25] H. A. Wheeler, "Formulas for the skin effect," *Proc. Innov., Res., Entrepreneurship*, vol. 30, no. 9, pp. 412–424, Sep. 1942, doi: 10.1109/JRPROC.1942.232015.

[26] N. D. Barrera et al., "Microwave characterization of Parylene C dielectric and barrier properties," in *Proc. IEEE 22nd Int. Conf. Solid-State Sensors, Actuators Micro-Syst. (Transducers)*, 2023.

[27] X. Ma et al., "A multistate single-connection calibration for microwave microfluidics," *IEEE Trans. Microw. Theory Techn.*, vol. 66, no. 2, pp. 1099–1107, Feb. 2018, doi: 10.1109/TMTT.2017.2758364.

[28] J. A. Jargon, C. J. Long, A. Feldman, and J. Martens, "Developing models for a 0.8 mm coaxial VNA calibration kit within the NIST microwave uncertainty framework," in *Proc. IEEE 94th ARFTG Microw. Meas. Symp.*, 2020, pp. 1–4, doi: 10.1109/ARFTG47584.2020.9071653.

[29] R. P. Von Metzen and T. Stieglitz, "The effects of annealing on mechanical, chemical, and physical properties and structural stability of Parylene C," *Biomed. Microdevices*, vol. 15, no. 5, pp. 727–735, 2013, doi: 10.1007/s10544-013-9758-8.

[30] J. M. Hsu, L. Rieth, R. A. Normann, P. Tathireddy, and F. Solzbacher, "Encapsulation of an integrated neural interface device with Parylene C," *IEEE Trans. Biomed. Eng.*, vol. 56, no. 1, pp. 23–29, Jan. 2009, doi: 10.1109/TBME.2008.2002155.

[31] W. Li, D. C. Rodger, E. Meng, J. D. Weiland, M. S. Humayun, and Y. C. Tai, "Flexible parylene packaged intraocular coil for retinal prostheses," in *Proc. IEEE Int. Conf. Micro-Technol. Med. Biol.*, 2006, pp. 105–108, doi: 10.1109/MMB.2006.251502.

[32] C. D. Lee and E. Meng, "Mechanical properties of thin-film Parylene–metal–Parylene devices," *Front. Mech. Eng.*, vol. 1, pp. 1–14, 2015, doi: 10.3389/fmech.2015.00010.

[33] C. Hassler, R. P. von Metzen, P. Ruther, and T. Stieglitz, "Characterization of Parylene C as an encapsulation material for implanted neural prostheses," *J. Biomed. Mater. Res. B Appl. Biomaterials*, vol. 93, no. 1, pp. 266–274, 2010, doi: 10.1002/jbm.b.31584.

[34] W. Li, D. C. Rodger, E. Meng, J. D. Weiland, M. S. Humayun, and Y. C. Tai, "Wafer-level parylene packaging with integrated RF electronics for wireless retinal prostheses," *J. Microelectromech. Syst.*, vol. 19, no. 4, pp. 735–742, 2010, doi: 10.1109/JMEMS.2010.2049985.

Jacob T. Pawlik (Member, IEEE) received the B.S. degree in chemistry with a minor in mathematics from Appalachian State University in Boone, NC, USA, in 2016, and the Ph.D. degree in materials chemistry from the University of North Carolina at Chapel Hill, Chapel Hill, NC, USA, in 2021. His graduate work focused on the discovery, synthesis, characterization, and implementation of novel materials for fluoride-ion batteries. He is currently a National Research Council Postdoctoral Chemist with the Guided Wave Electromagnetics Group working on microwave microfluidic measurements of electrochemical systems. In 2021, he joined as a Postdoctoral Associate with the National Institute of Standards and Technology, Professional Research Experience Program, University of Colorado Boulder, Boulder, CO, USA. His work focuses on microwave measurements of polymers relevant to implantable devices.

Nikolas D. Barrera received the B.S. degree in biomedical engineering from the University of Michigan, Ann Arbor, MI, USA, in 2019. He is currently working toward the Ph.D. degree in biomedical engineering with the University of Southern California, Los Angeles, CA, USA. His doctoral research is focuses on the development of flexible neural interfaces. Since 2021, he has been an Intern with the National Institute of Standards and Technology as a graduate student associate studying dielectric properties of polymers in medical device applications.

Eugene J. Yoon received the B.S. degree in chemical and biomolecular engineering from Johns Hopkins University, Baltimore, MD, USA, in 2015, and the M.S. and Ph.D. degrees in biomedical engineering from the University of Southern California, Los Angeles, CA, USA, in 2017 and 2021, respectively. His graduate work focused on the Parylene C bioMEMS for implantable devices with electrochemical interfaces. He has held research fellowship positions with Interuniversity Microelectronics Centre, Leuven, Belgium, and the National Institute of Standards and Technology, Boulder, CO, USA. He was a Microfabrication Engineer with Science Corporation in Alameda, Alameda, CA, USA. He is currently a nanofabrication lab operations Engineer with the O'Brien Nanofabrication Laboratory, University of Southern California, Los Angeles, CA, USA.

James C. Booth (Member, IEEE) received the B.A. degree in physics from the University of Virginia, Charlottesville, VA, USA, in 1989, and the Ph.D. degree in physics from the University of Maryland, College Park, MD, USA, in 1996, where the subject of his dissertation was Novel measurements of the frequency dependent microwave surface impedance of cuprate thin film superconductors. He has been a Physicist with the National Institute of Standards and Technology, Boulder, CO, USA, since 1996, originally as an NRC Postdoctoral Research Associate during 1996–1998. He is currently a Leader of the RF Electronics Group, Communications Technology Laboratory. His research at NIST is focuses on quantifying the microwave properties of new electronic materials and devices, including piezoelectric, ferrite, magneto-electric, and superconducting materials, and linear and nonlinear measurements and modeling of analog components, such as transmission lines and filters. Dr. Booth was the recipient of the Department of Commerce Bronze Medal in 2015 for the development and application of measurements to determine electrical properties of thin-film materials over a range of frequencies from a few hertz to the terahertz regime.

Christian J. Long received the B.S. and Ph.D. degrees in physics from the University of Maryland at College Park, College Park, MD, USA, in 2004 and 2011, respectively. His doctoral research focused on the development of both microwave near-field scanning probe microscopy techniques and new methods to analyze data from combinatorial materials experiments. From 2012 to 2015, he was a Postdoctoral Researcher with the National Institute of Standards and Technology (NIST), Gaithersburg, MD, USA, where he focused on techniques for characterizing nanoscale materials. In 2016, he joined the staff with NIST, Boulder, CO, USA, where he currently leads a project on the development of on-chip standards for microwave and mm-wave calibration.

Nathan D. Orloff (Senior Member, IEEE) received the B.S. (Hons.) and Ph.D. degrees in physics from the University of Maryland at College Park, College Park, MD, USA, in 2004 and 2010, respectively. His doctoral thesis involved the study and extraction of microwave properties of Ruddlesden-Popper ferroelectrics. In 2011, he joined the Department of Bioengineering, Stanford University, Stanford, CA, USA, as a Dean's Postdoctoral Fellow with Prof. I. Riedel-Kruse. In 2013, he joined the Materials Measurement Laboratory, National Institute of Standards and Technology (NIST), Gaithersburg, MD, USA, as a Rice University Postdoctoral Fellow with Prof. M. Pasquali. In 2014, he joined the newly formed Communications Technology Laboratory, NIST, to lead the Microwave Materials Project.

Dr. Orloff was the recipient of the 2004 Martin Monroe Undergraduate Research Award, 2006 CMPS Award for Excellence as a Teaching Assistant, 2010 Michael J. Pelczar Award for Excellence in Graduate Study, and 2015 Communications Technology Laboratory Distinguished Associate Award.

Ellis Meng (Fellow, IEEE) received the B.S. degree in engineering and applied science and the M.S. and Ph.D. degrees in electrical engineering from the California Institute of Technology (Caltech), Pasadena, CA, USA, in 1997, 1998, and 2003, respectively. Since 2004, she has been with the University of Southern California, Los Angeles, CA, USA, where she was the Viterbi Early Career Chair and then the Department Chair. She is currently the Shelly and Ofer Nemirovsky Chair of Convergent Biosciences and a Professor of biomedical engineering and electrical and computer engineering. She is also the Vice Dean for Technology Innovation and Entrepreneurship. Her research interests include bioMEMS, implantable biomedical microdevices, microfluidics, multimodality integrated microsystems, and packaging. She is a Fellow of ASME, BMES, AIMBE, and NAI. She was the recipient of the NSF CAREER Award, Wallace H. Coulter Foundation Early Career Award, 2009 TR35 Young Innovator Under 35, Viterbi Early Career Chair, ASEE Curtis W. McGraw Research Award, 2018 IEEE Engineering in Medicine and Biology Society Technical Achievement Award, and 2019 IEEE Sensors Council Technical Achievement Award. She is currently the VP of Technical Activities for IEEE Engineering in Medicine and Biology Society.

Angela C. Stelson (Member, IEEE) received the B.S. degree in physics, mathematics, and political science from the University of Oregon, Eugene, OR, USA, in 2012, and the Ph.D. degree in materials science and engineering from Cornell University, Ithaca, NY, USA, in 2017. Her graduate work focused on the electric-field directed assembly of colloids for photonic crystals. In 2017, she joined the National Institute of Standards and Technology as a National Research Council Fellow. She is currently with the RF Electronics Group developing new microwave microfluidics measurement techniques for medical diagnostics, pharmaceutical, and materials science applications.